Microfluid Nanofluid (2017) 21:32
DOI 10.1007/s10404-017-1863-1

RESEARCH PAPER

Permeability model of micro-metal foam with surface micro-roughness

X. H. Yang[1,2] · S. Y. Song[1] · C. Yang[3] · W. J. Hu[4] · F. S. Han[5] · L. W. Jin[1] · T. J. Lu[2,6]

Received: 15 October 2016 / Accepted: 17 January 2017 / Published online: 16 February 2017

Abstract We present an analytical model capable of predicting permeability for isotropic and fully saturated micro-open-cell metal foam with surface modified by micro-rods (30–50 μm). The analytical model is based on the pore-scale volume-averaging approach and the assumption of piece-wise plane Poiseuille flow with the reconstructed three-dimensional cubic unit cell having cylindrical micro-rods synthesized on the cell walls. Both of the metal foam structure and the randomly distributed micro-rods are assumed to be periodic. The proposed model includes both the macroscopic and microscopic parameters that characterize the metal foam as well as the micro-roughness. The effects of micro-rod radius, height and interval on permeability and tortuosity are examined. To validate the present analytical model, experimental results are employed and good agreement is found. Results demonstrate that the micro-rods synthesized on the cell walls significantly decrease the permeability of the micro-foam. The increase in micro-rod radius/height or decrease in rod interval makes the metal foam surface rougher and thus decreases the foam permeability.

Keywords Permeability · Micro-roughness · Open-cell foam · Unit cell modeling · Analytical model

1 Introduction

With ultra-low density, high surface area to volume ratio, relatively low cost, and especially fluid mixing ability, high porosity open-cell metal foams are attractive for a variety of engineering applications such as porous catalyst (Burke et al. 2013; He et al. 2011), chemical engineering (von Rickenbach et al. 2014), microelectronics cooling (Lu et al.

This paper was significantly revised based on the short version, which was presented at the MNLOC 2016, June 10-12, 2016, Dalian, China and submitted to the special issue "S.I.: Microfluidics, Nanofluidics and Lab-on-a-Chip".

This article is part of the topical collection "2016 International Conference of Microfluidics, Nanofluidics and Lab-on-a-Chip, Dalian, China" guest edited by Chun Yang, Carolyn Ren and Xiangchun Xuan.

✉ L. W. Jin
lwjin@xjtu.edu.cn

✉ T. J. Lu
tjlu@xjtu.edu.cn

[1] Group of the Building Energy and Sustainability Technology, School of Human Settlements and Civil Engineering, Xi'an Jiaotong University, Xi'an 710049, China

[2] Moe Key Laboratory for Multifunctional Materials and Structures, Xi'an Jiaotong University, Xi'an 710049, China

[3] School of Mechanical and Aerospace Engineering, Nanyang Technological University, 50 Nanyang Avenue, Singapore 639798, Singapore

[4] Beijing Municipal Key Lab of Heating, Gas Supply, Ventilating and Air Conditioning Engineering, Beijing University of Civil Engineering and Architecture, Xicheng District, Beijing 100044, China

[5] Key Laboratory of Materials Physics, Institute of Solid State Physics, Chinese Academy of Sciences, Hefei 230031, Anhui, China

[6] State Key Laboratory for Strength and Vibration of Mechanical Structures, School of Aerospace, Xi'an Jiaotong University, Xi'an 710049, China

1998), fuel cells (Kumar and Reddy 2003; Tawfik et al. 2007), petroleum engineering (Cai et al. 2012), gasification (Lefebvre et al. 2008), refrigeration (Yang et al. 2016) and biomedical applications (Zhang 2011). Permeability is one of the key parameters describing fluid transport phenomena for porous media and is also one of the designing considerations for those applications (Bacchin et al. 2014; Liu et al. 2016; Lv et al. 2014). In contrast to conventional porous media (e.g., packed beds) for enhancing fluid–solid contact (Saini et al. 2015) (Sen et al. 2012), the extremely large surface area within unit volume (namely specific area) with low pressure drop is more effective in intensification of hydrodynamic interactions between fluid and solid phases (Edouard et al. 2008; Galindo-Rosales et al. 2012; Lacroix et al. 2007). It is expected to have a better performance with a higher specific area. Recently, Ren et al. (2013) further enlarged the specific area of aluminum foam through synthesis of ZnO micro-rods (30 μm) on the foam surface walls. They experimentally found that both the flow resistance and sound absorption coefficient were significantly increased. At present, however, the physical insight into the fluid transport in porous metal foams with surface microroughness and analytical model for the key parameter—permeability for describing fluid transport phenomena have not been investigated in the open literature. The present study therefore aims to address this issue through theoretical analysis at micro-pore scale.

Microstructures of porous media significantly affect the fluid transport phenomena and transport properties, e.g., permeability (Keh and Hsu 2009; Mu et al. 2008; Straughan and Harfash 2013). To investigate the mass transfer and model transport process, two kinds of theoretical approaches have been developed. One is fractal analysis. This approach treats porous media as self-consistent and assumes that their geometrical characteristics, e.g., pore size distribution follow the fractal scaling laws. This kind of porous media are commonly called fractal porous media. The complicated flow paths are also assumed to be bundles of tortuous capillaries. By determining the fractal dimensions for size distributions of capillaries and flow tortuosity, the permeability of porous media can be readily achieved. Prof. Yu's research group (Cai et al. 2010a, b, 2015; Cai and Yu 2010; Yang et al. 2015; Yu 2008; Yu and Cheng 2002; Yu et al. 2002) has concentrated on the fractal analysis for transport properties over 20 years, and they have contributed significantly to the development in this area. They systematically characterized porous media in deriving theoretical models of fractal dimension for pore volume (Yu and Li 2004) and pore size (Cai and Yu 2010; Yu and Cheng 2002) in porous media with complicated structures. Based on the theoretical analysis for characterizing fractal porous media, fractal permeability model (Yu and Cheng 2002; Yu et al. 2002) was rigorously derived and has been shown to be valid not only for particle-like porous media but also for fibrous media. More detailed work can be referred to the critical summaries in merit of basic concepts and the advances in fluid transport in fractal porous media (Cai et al. 2015; Yu 2008).

The other approach assumes that the pore microstructures of real porous media are periodic. There is a unit cell that is microscopically large enough to possess all the topological and morphological characteristics that the bulk porous medium has; and the flow features in pore scale can represent macroscopic flow condition (Shou et al. 2014; Yang et al. 2013a, b). Poiseuille and Stokes flows are commonly assumed at pore scale, and volume-averaging is applied on the inner pore surfaces within a simple geometrical unit cell to solve the pore-scale Navier–Stokes equations.

Depois and Mortensen (Despois and Mortensen 2005) took packed spheres to represent the microstructure of open-cell metal foam. They derived an analytical model for predicting permeability of an open-cell aluminum foam on the geometrical basis of packed beds. Although the model predictions showed good agreement with experimental results for foam permeability, their assumed microstructure (packed spheres) for porous foam seems far from that of the real topological structure of aluminum foam and the transport physics between the two porous media are significantly different. A more appropriate geometrical model was developed by Du Plessis and his co-workers (Du Plessis et al. 1994, 2010; Du Plessis and Masliyah 1988; Du Plessis and Woudberg 2008; Fourie and Du Plessis 2002) and continuous investigations on the cubic geometry have been conducted. Volume-averaged Navier–Stokes equations were solved within the cubic unit cell, based on the assumed Poiseuille flow on the cubic surface. Their model showed satisfactory predictions for permeability of open-cell metal foam only in the high porosity range (0.973–0.978). Over-predicted results for permeability were found in a larger range of porosity (0.90–0.97), and this was attributed to the lack of node sizes at the ligaments intersection, which was thought to increase the flow tortuosity. Bhattacharya et al. (2002) further modified and characterized the cubic geometry unit cell based on the measured microstructural parameters of the real metal foam. An empirical correlation for microstructural parameters (node size) was introduced to modify the flow tortuosity within the cubic unit cell. Their model predictions on the foam permeability and inertial coefficient were in quite good agreement with their experimental results. However, Ahmed et al. (2011) found that the model for tortuosity increased with foam porosity, which agreed poorly with experimental data. Through further modification and extension, their attempts were successfully in predicting permeability of open-cell metal foams. Besides, the classical Kozeny-Carmen model

originated for predicting the permeability of packed beds was also employed to estimate fluid transport in open-cell metal foams through modifications and extensions (Dukhan 2006; Hooman and Dukhan 2013; Lacroix et al. 2007). The empirical constants in Kozeny-Carmen's model were fitted through experimental results.

Among the above-mentioned theoretical models, little effort has been made to include surface micro-roughness. To our best knowledge, only recent studies by Yu' group (Cai et al. 2010a; Yang et al. 2015) considered the micro-roughness effect on fluid transport in porous media. Cai et al. (2010a) systematically characterized the degree of roughness or disorder of particle surface for roughed particles in porous media. A fractal dimension for roughness height (*RH*) was introduced and was later exploited by Yang et al. (2015) to develop the permeability model for porous media with roughed surface. They developed a fractal model for predicting the permeability of mono- and bi-dispersed porous media with roughed surfaces, and their model showed good agreement with experimental results. Although these theoretical works cannot be directly employed to model fluid transport in open-cell metal foam with surface micro-roughness (due to the topological difference between mono-/bi-dispersed porous media and open-cell metal foam), these investigations significantly advance the development of fluid transport in porous media and their concepts. In this work, a theoretical model for predicting the permeability of open-cell metal foam with surface micro-roughness is developed, which is based on the idealized microstructure—cubic unit cell with micro-cylindrical rods on the surface. For validation, model predictions for permeability are compared with experimental results. The effects of length, radius and distribution density of micro-rods grown on the foam inner surface upon permeability are also discussed.

2 Model developments

2.1 Fluid flow in a representative unit cell of micro-foam with smooth surface

The notoriously complicated microstructures of open-cell metal foam deteriorate the theoretical analysis of fluid transport in the precise microstructure. It is recognized that the periodical distributions of cubic unit cells (see Fig. 1) can provide satisfactory description of metal foam microstructure and corresponding fluid transport in open-cell metal foams (Ahmed et al. 2011; Bhattacharya et al. 2002; Du Plessis and Masliyah 1988; Du Plessis and Woudberg 2008; Du Plessis et al. 1994; Fourie and Du Plessis 2002; Yang et al. 2014). Therefore, an idealized cubic unit cell (UC) shown in Fig. 1 is selected to represent real foam

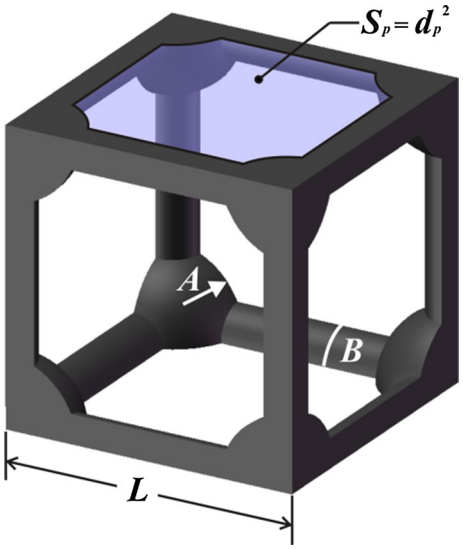

Fig. 1 Open-cell Al foams modeled with a cubic unit cell for deriving permeability model

microstructure and theoretical analysis is performed based on the cubic UC.

Rigorously speaking, there exists velocity distribution at micro-pore scale for open-cell metal foam and it has a notoriously complicated mathematical expression. Even if the simplified cubic UC is employed, the explicitly mathematical expression for this velocity distribution is still too difficult to derive. Commonly, volume-averaging within a representative UC is performed and representative mean velocity—volume-averaged $\langle v \rangle_f$ is chosen. The volumetric flow rate through the present UC with a cross-sectional area S_p can be separately calculated as $v_p S_p$ and $\langle v \rangle_f L^2$. Hence, the average pore velocity v_p takes:

$$v_p S_p = \langle v \rangle_f L^2 \tag{1}$$

where v_p is the average pore velocity in a longitudinally oriented pore, L and S_p are, respectively, the length and pore window area of the cubic UC. It was suggested (Du Plessis et al. 1994; Fourie and Du Plessis 2002) that the flow tortuosity within a UC is defined as the ratio of total winding path to the length of the UC. With the total winding path expressed as $L_e = V_f / S_p$, the tortuosity becomes,

$$\chi = \frac{L_e}{L} = \frac{V_f / S_p}{L} = \frac{\phi V_t}{S_p L} = \frac{\phi L^2}{S_p} \tag{2}$$

where χ is the flow tortuosity within a UC, ϕ denotes the void fraction (porosity) for a UC, L_e and L are, respectively, the total winding path and the length of the cubic UC, V_f and V_t are the volume for the saturating fluid and for the total cubic UC, respectively, and S_p denotes

the open-pore area (pore window size). Substitution of Eq. (2) into Eq. (1) yields

$$v_p = \langle v \rangle_f \frac{\chi}{\phi} \tag{3}$$

Du Plessis et al. (1994) and Fourie and Du Plessis (2002) analyzed the topological features of the cubic UC and employed the pore-scale volumetric averaging theory to analyze the fluid flow behavior in the representative cubic UC for open-cell metal foams with high porosity. They proposed an analytical expression between the volume-averaged pressure gradient of fluid flow through a cubic UC and the corresponding viscous shear factor, expressed as:

$$\nabla \langle p \rangle_f = \frac{\mu \langle v \rangle_f}{\phi} f \tag{4}$$

where $\langle p \rangle_f$ and $\langle v \rangle_f$ are the volume-averaged pressure and velocity, ϕ is the foam porosity, f is the viscous shear factor. For the low Reynolds number range, namely the Darcy flow regime, the viscous shear factor can be approximated as the drag force (f_v) in a UC (see Fig. 1) with a frontal area L^2 and a depth L (Du Plessis et al. 1994; Fourie and Du Plessis 2002):

$$f_v = -\phi \nabla \frac{\langle p \rangle_f}{\phi} L^3. \tag{5}$$

As suggested by White and Corfield (2006), the drag force can be written as a function of friction coefficient, expressed as:

$$f_v = \frac{C_{D,v} \rho_f v_p^2 S_{sf}}{2} \tag{6}$$

where $C_{D,v}$ is the friction coefficient, ρ_f is the fluid density, and S_{sf} denotes the wetted surface area of the cubic UC in Fig. 1.

Substituting Eqs. (3), (5) and (6) into Eq. (4), we get the drag force as:

$$f_v = \frac{\rho_f \chi^2 S_{sf}}{2\mu\phi^2 L^3} C_{D,v} \langle v \rangle_f \tag{7}$$

It is assumed that the drag force equals to the viscous shear factor within the cubic UC (Du Plessis et al. 1994; Fourie and Du Plessis 2002), namely Eq. (7) equals to Eq. (4), resulting to

$$\frac{\nabla \langle p \rangle_f}{\phi} = -\frac{\rho_f \chi^2 S_{sf}}{2\phi^3 L^3} C_{D,v} \langle v \rangle_f^2 \tag{8}$$

For the friction coefficient, Du Plessis and his coworkers (Du Plessis et al. 1994; Fourie and Du Plessis 2002) linked the hydrodynamic stresses at the solid–fluid interface of the UC to the plane Poiseuille flow at a mean pore velocity. Then, the friction coefficient can be expressed as:

$$C_{D,v} = \frac{12\mu\phi}{\rho_f v_p d_p} \tag{9}$$

where d_p is the equivalent diameter of the UC window and it is defined as $d_p^2 = S_p$.

Combining Eqs. (8–9) and Darcy's law for the pressure drop in a volume-averaged form gives

$$\frac{\nabla \langle p \rangle_f}{\phi} = -\frac{\mu \langle v \rangle_f}{\phi K} \tag{10}$$

Therefore, an analytical expression for the viscous permeability (K) can be obtained:

$$\frac{K}{L^2} = \frac{\phi d_p L}{6\chi S_{sf}} \tag{11}$$

where the foam porosity ϕ and pore size L are usually provided by the manufacturer, the flow tortuosity χ, the equivalent diameter d_p and the wetted surface area S_{sf} can be calculated according to the topological characteristics of the cubic unit cell.

2.2 Description of micro-foam surface morphology

Open-cell metallic foams have porous cellular structure consisting of inner-connected pores and fibers-made skeleton, as shown in Fig. 2a. The inner-connected aluminum ligaments join together, and there forms a joint that has a bigger size than the ligament thickness, namely node. Figure 2b depicts the SEM image of a single ligament out of the whole metal foam sample. It can be observed that the ligament has a prism shape, and its surface is not absolutely smooth, namely there exists some micro-tubers on the ligament surface. This is mainly due to the fabrication routine of direct foaming, during which the foaming gas in the molten slurry moves freely, forming eventually inner-connected porous matrix (Weaire and Hutzler 2001). The micro-tubers on the ligament surface are formed due to the sudden cooling as the gas escapes from the molten slurry.

Compared with the original metal foam surfaces, the ligament surfaces are all covered with ZnO micro-rods (see Fig. 2c) synthesized by the hydrothermal method (Ren et al. 2013). It is obvious that the ligament surface is much rougher than that of the original metal foam. The micro-rods with a hexagonal cross section, a side length of 2.5 μm and the height of around 30 μm are densely distributed and are in disordered pattern.

To model the fluid transport in such kind of porous media with surface micro-roughness, the original cubic UC (Fig. 1) needs to be modified. In the present study, the micro-roughness is treated by micro-cylindrical rods with a height of h and radius of r for simplicity. The periodically distributed micro-cylindrical rods are added on the inner surface of the solid ligaments and spherical nodes. As shown in Fig. 3a, a cubic UC consisting of twelve ligaments (identical length L and ligament radius B) with a spherical node (diameter is A) at the joint is employed as

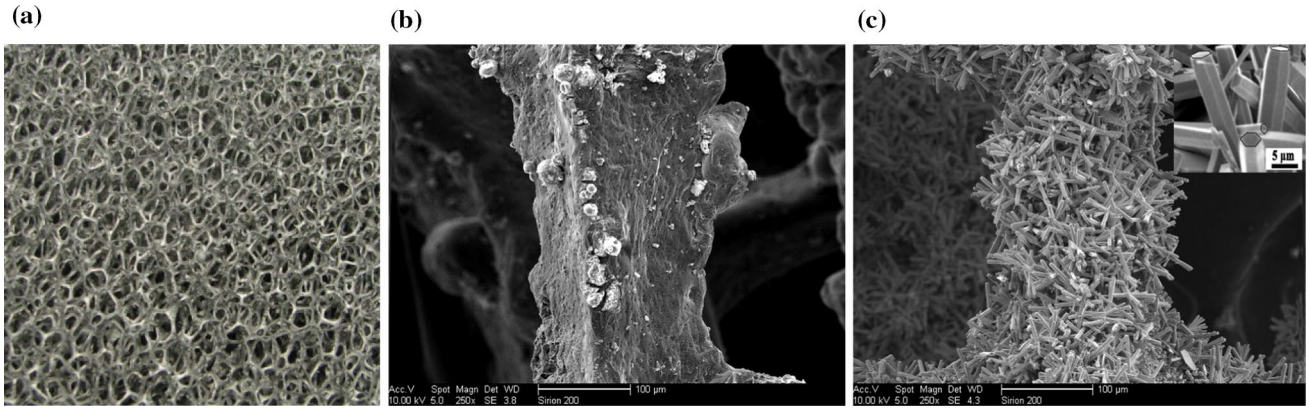

Fig. 2 Open-cell Al foams samples: **a** image of Al foam without surface micro-roughness (original metal foam); **b** SEM image for the ligament of the original metal foam; **c** SEM image for the ligament covered with micro-rods (Ren et al. 2013)

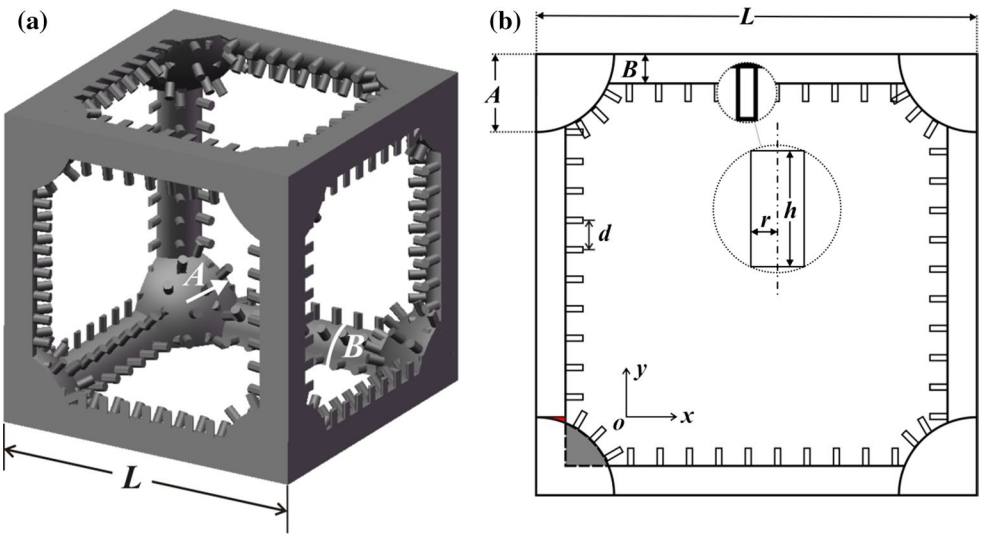

Fig. 3 Modified cubic UC accounting for the surface micro-roughness: **a** 3D unit cell; **b** top view. Micro-cylinders in periodic arrangement are selected to represent the real micro-rods in disordered distribution

the topological basis for modeling fluid transport in metal foam. It should be noted here that the micro-roughness in metal foam specimen (Fig. 2c) is densely packed on the surface, while the micro-cylindrical rods are loosely packed for the cubic UC; this is mainly to show clearly the distribution pattern and qualitatively geometrical characterization for the micro-rods.

2.3 Unit cell characterization

The present permeability model (Eq. 11) requires characterizing the cubic UC with surface micro-roughness. The following sections introduce the quantifications of the specific area, window size, tortuosity and porosity for metal foam. Given the topological nature of the cubic UC, the structure is divided in three parts: nodes, cylindrical ligaments and the surface micro-rods.

There are eight nodes in the cubic UC, and each has a superficial area of $0.5\pi A^2$. Hence, the total superficial area inside the UC is $4\pi A^2$. Considering the fact that there are some areas covered by the ligaments (joint part), the covered area (S_{covered}) should be subtracted. The covered area, spherical crown in Math, can be determined by

$$S_{\text{covered}} = 12\pi A(A - \sqrt{A^2 - B^2}) \tag{12}$$

where A and B are, respectively, the radius of the node and cylindrical ligament and the node size A is typically 1.5 times of the ligament size B. The superficial area with smooth surface is

$$S_{\text{node}} = S_{\text{sphere}} - S_{\text{covered}} = 4A^2\pi - 12\pi A(A - \sqrt{A^2 - B^2}) \tag{13}$$

There are twelve ligaments in the UC, and each one is a 1/4 cylinder with the length of $(L - (2\sqrt{A^2 - B^2}))$. So we have,

$$S_{\text{ligament}} = 6(L - (2\sqrt{A^2 - B^2}))B\pi \tag{14}$$

For characterizing the micro-rods, we introduce a new parameter, distribution density ω that is defined as the number of micro-rods within unit area, equaling to d^{-2} (d is the interval of the micro-rods (see Fig. 3b). Then, the total micro-rods can be readily quantified by ωS_{smooth} in the cubic UC. Each micro-cylinder has a superficial area of $2\pi hr$. So we have the increased superficial area by micro-rods as

$$S_{\text{roughness}} = 2hr\pi\omega S_{\text{smooth}} \tag{15}$$

where S_{smooth} denotes the total superficial area within a UC without micro-roughness and it can be quantified by

$$S_{\text{smooth}} = S_{\text{node}} + S_{\text{ligament}} = 4A^2\pi - 12\pi A(A - \sqrt{A^2 - B^2}) + 6B\pi(L - 2\sqrt{A^2 - B^2}) \tag{16}$$

Then, the total superficial area that a cubic UC has can be obtained as

$$S_{sf} = S_{\text{node}} + S_{\text{ligament}} + S_{\text{roughness}} = 4A^2\pi - 12\pi A(A - \sqrt{A^2 - B^2}) + 6B\pi(L - 2\sqrt{A^2 - B^2}) + 2hr\pi\omega S_{\text{smooth}} \tag{17}$$

Now, we are going to derive an expression for the equivalent pore diameter d_p of the cubic UC. Figure 3b depicts the top view of the cubic UC; the window size can be calculated through the subtraction of node, ligament as well as the micro-rods. To distinguish the superficial area with the lateral area, here we use the symbol "T" to represent the lateral area. The area for the small node T_{node} in gray color takes the form as

$$T_{\text{node}} = 4\left(\frac{1}{2}A^2\left(\frac{\pi}{2} - 2\arcsin\left(\frac{B}{A}\right)\right) - \left(\sqrt{A^2 - B^2} - B\right)B\right) \tag{18}$$

For the ligament area in a lateral surface, we have

$$T_{\text{ligament}} = 4LB - 4B^2 \tag{19}$$

As mentioned above, ω denotes the number of micro-rods within a unit area; here, we use $\sqrt{\omega}$ to quantify the linear distribution density of the micro-rods. The perimeter of a lateral window is

$$C=4\left(L - 2\sqrt{A^2 - B^2}\right) + 4A\left(\frac{\pi}{2} - 2\arcsin\frac{B}{A}\right) \tag{20}$$

Therefore the total area that the micro-rods have can be obtained as a function of the linear distribution density,

$$T_{\text{rough}} = C\sqrt{\omega}\cdot 2rh = 48\left(\left(L - 2\sqrt{A^2 - B^2}\right) + A\left(\frac{\pi}{2} - 2\arcsin\frac{B}{A}\right)\right)\sqrt{\omega}rh \tag{21}$$

Summation of these areas yields the lateral area for a cubic UC,

$$T = T_{\text{node}} + T_{\text{ligament}} + T_{\text{rough}} = 4LB - 4B^2 + 2A^2\left(\frac{\pi}{2} - 2\arcsin\left(\frac{B}{A}\right)\right) - 2B\left(\sqrt{A^2 - B^2} - B\right) + 4\sqrt{\omega}rh\left(\left(L - 2\sqrt{A^2 - B^2}\right) + A\left(\frac{\pi}{2} - 2\arcsin\frac{B}{A}\right)\right) \tag{22}$$

and then the equivalent pore diameter d_p can be readily determined through the following equation

$$d_p = \sqrt{S_p} = \sqrt{L^2 - T} \tag{23}$$

The characteristic elements (cube) have eight vertexes, twelve edges and six surfaces. The following calculations will be performed separately for the nodes at the vertexes, the ligaments at the edges and the roughness distributed on the surface of the inside surface to determine the porosity of the current cubic cell. We take the division strategy of summation of the entire node, the irregular part (in red of Fig. 3b) and the straight ligament. The volume of the entire node can be readily obtained via the volume formula of the sphere as,

$$V_{\text{smooth-node}} = \frac{4}{3}A^3\pi \tag{24}$$

There are twelve straight cylindrical ligaments in a cubic UC, and each has the length of $(L - 2A)$. The total volume of these ligaments is calculated by

$$V_{\text{straight cylinder}} = 3(L - 2A)B^2\pi \tag{25}$$

The volume of the irregular area (in red of Fig. 3b) can be obtained by integration,

$$V_{\text{irregular}} = 6\int_{\sqrt{A^2 - B^2}}^{A}\left[\left(B^2\pi\right) - \left(A^2 - y^2\right)\pi\right]\mathrm{d}y \tag{26}$$

For the micro-rods, each has a volume of πhr^2. With the total number the micro-cylinder $S\omega$, we have their total volume

$$V_{\text{rough - roughness}} = S\omega \times hr^2\pi \tag{27}$$

Summation of each volume for solid phase in the current cubic UC then yields

$$V_{\text{solid}} = \frac{4}{3}A^3\pi + S\omega hr^2\pi + (3L - 6A)B^2\pi + 6\left[\left(B^2\pi(A - \sqrt{A^2 - B^2})\right) - \pi\left(\frac{2}{3}A^3 - \frac{2}{3}A^2\sqrt{A^2 - B^2} - \frac{1}{3}B^2\sqrt{A^2 - B^2}\right)\right] \tag{28}$$

and now the porosity can be obtained

$$\phi = \frac{V_{\text{solid}}}{V_t} \tag{29}$$

where the total volume of the cubic UC V_t equals to L^3.

Hereto, all the parameters required for calculating the foam permeability are provided. Substitution of Eqs. (2), (16), (17), (22), (23), (28), (29) into Eq. (11) yields the final expression for the permeability of open-cell metal foam with surface micro-roughness. Due to the very complicated expression for the permeability, the final mathematical formula is not explicitly presented here. Its value and variation with microstructural parameters will be discussed in the following sections.

3 Results and discussion

3.1 Model validation

To validate the present analytical model, experimental results are employed for comparison. Table 1 shows the detailed parameters for the specimens and their permeability comparison between the model prediction and the experimental measurements. Before surface modification, the four specimens have the same porosity of 0.92 and different pore diameters of 1 and 2.5 mm. After surface modification, the four specimens can be categorized into two groups: one is metal foam with surface covered by ZnO micro-rods (see Fig. 2c) and the other is that covered by Co_3O_4 micro-rods (see Fig. 4). ZnO micro-rod looks like prism with hexagonal cross-sectional shape. The height of ZnO micro-rod is about 30 μm, and the side length is about 2.5 μm (Ren et al. 2013). Recalling that the micro-cylindrical shape was assumed in the model development; therefore, an equivalent circular radius of 4.77 μm was employed to calculate the metal foam permeability. Co_3O_4 micro-rod has a needle-like shape with a radius of 5 μm, and its height is varied from 30–50 μm with processing time (2–10 h). This can be verified from the SEM images for Co_3O_4 micro-rods after processed by 2, 6 and 10 h.

For open-cell Al foams with surface covered by micro-rods (ZnO or Co_3O_4), Table 1 compares the analytically predicted permeability using the present model with the

Table 1 Comparison of predicted permeability of open-cell metal foam (roughed surface) with experimental measurements (Ren et al. 2013, 2014)

Foam sample	ϕ	L (mm)	r (μm)	h (μm)	K (pred) (m^2)	K (expt) (m^2)	Relative error (%)
ZnO micro-rods	0.92	1	4.77	30	8.02×10^{-9}	7.99×10^{-9}	0.33
Co_3O_4 (2 h)	0.92	2.5	5	30	9.58×10^{-9}	8.82×10^{-9}	8.67
Co_3O_4 (6 h)	0.92	2.5	5	40	6.92×10^{-9}	6.61×10^{-9}	4.75
Co_3O_4 (10 h)	0.92	2.5	5	50	5.38×10^{-9}	5.83×10^{-9}	7.73

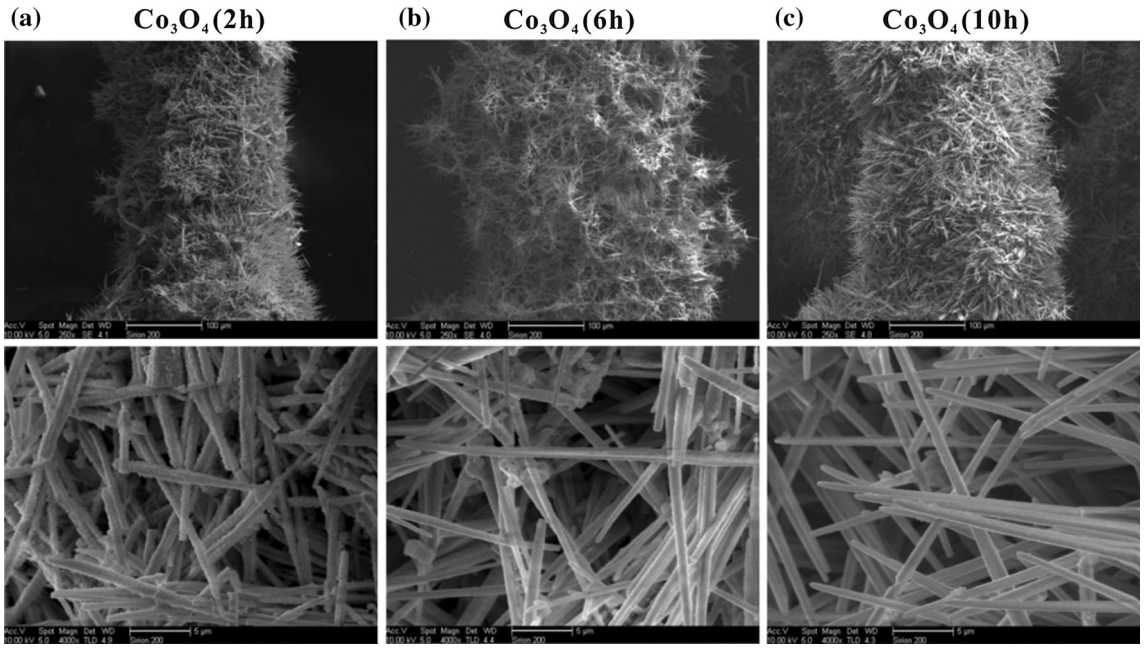

Fig. 4 Open-cell metal foams with superficially grown Co_3O_4 micro-rods under different growing time: **a** 2 h; **b** 6 h; **c** 10 h (Ren et al. 2014)

experimental data from the open literature (Ren et al. 2013, 2014). It shows that the analytical model predicts accurately the permeability for the metal foams with surface covered with micro-rods, where the root-mean-square (RMS) deviations from the experimental data are within 9% for using ZnO or Co_3O_4 as the micro-roughness. The permeability of the metal foam with micro-Co_3O_4 (2 h) is a little bit higher than that with micro-ZnO rods, due mainly to the bigger pore diameter for the metal foam with ZnO micro-roughness (see Table 1). Besides, for the three samples processed by Co_3O_4, a decreasing trend is observed as increasing rod height. For instance, the permeability is decreased by 43.89% when the processing time is increased from 2 to 10 h.

3.2 Dependence of permeability on porosity

Figure 5a–c separately shows the dependence of permeability on the metal foam porosity with different micro-parameters (radius, height and interval). It was reported that the typical porosity of engineering-utilized open-cell metal foams ranges from 0.88 to 0.99. Therefore, the same metal foam porosity is selected for investigation. For all the three groups (Fig. 5a–c) of data, the fixed pore diameter ($L = 1$) before surface modification is assumed. As can be observed in Fig. 5a–c, the permeability (in dimensionless form) of open-cell metal foams with/without surface micro-rods is monotonically increased with metal foam porosity. For instance, as porosity is increased from 0.90 to 0.98, an increment ratio of 3.45 is observed for the metal foam without micro-roughness and 4.04 is obtained for that with micro-rods having a radius of 5 μm, a height of 30 μm and an interval of 13 μm. It may be explained as follows. It is easier for convective flow to travel in porous media having larger pores for a given porosity, leading to higher porosity (for a given pore size). It is intuitive that with the porosity increased while maintaining pore size, the ligaments constructing the pore structure, are thinned, thereby reducing flow resistance and tortuosity. As a result, a higher permeability value exists.

For a given porosity, the involvement of surface micro-roughness significantly reduces the metal foam permeability. Figure 5a depicts the metal foam permeability versus foam porosity as given micro-rod height of 30 μm and interval of 13 μm at different micro-radii. With increasing the rod radius from 1 to 5 μm as shown in Fig. 5a, the permeability is further reduced. For example, for a selected porosity of 0.94, the reduction ratio of permeability is varied from 53.66 to 84.03%. This reduction in metal foam permeability is mainly due to the increased flow tortuosity caused by the increased rod radius. The bigger the micro-rod, the higher extent of tortuosity the flow will be. As a result, the bigger the micro-rod, the lower the foam permeability will be. Figure 5b demonstrates the metal foam

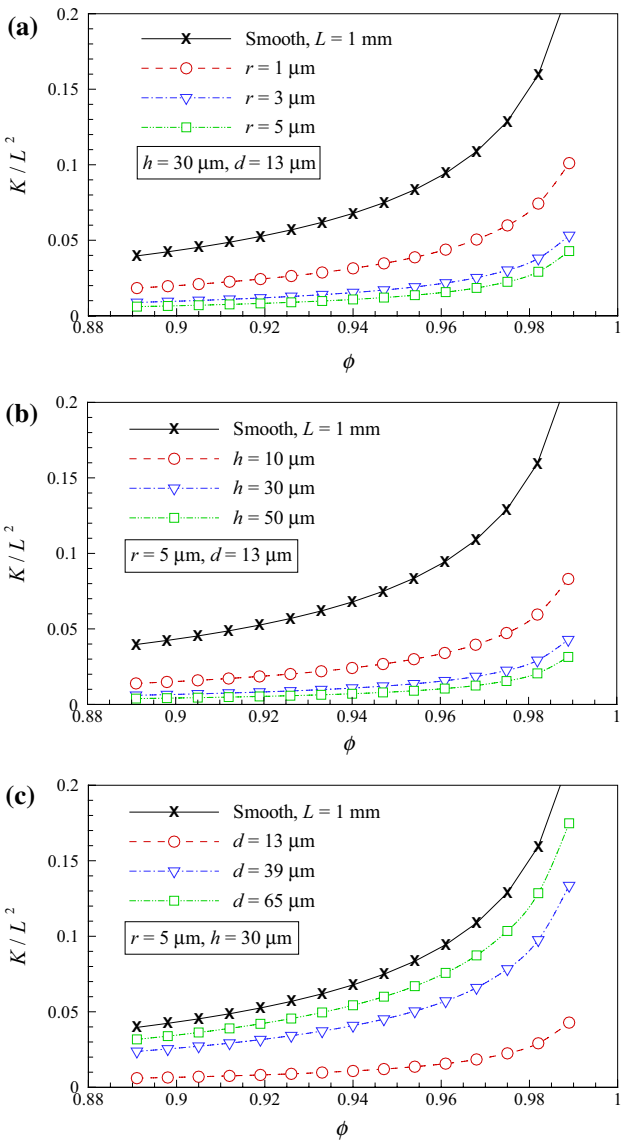

Fig. 5 Porosity dependence of permeability of open-cell Al foams: effect of micro-rod parameters on **a** rod radius; **b** rod height; **c** rod interval (distribution density)

permeability versus foam porosity with given micro-rod radius of 5 μm and interval of 13 μm at different micro-heights. Similar trend is observed as changing rod radius for a given porosity when increasing micro-rod height from 10 to 30 μm. As for the effect of micro-rod interval, as shown in Fig. 5c the smaller the interval, the denser the rods are distributed. Thus, the lower the foam permeability will be.

3.3 Effect of micro-rod height-to-radius ratio

In this section, the effect of micro-rod height-to-radius ratio on the macroscopically geometrical parameters (specific

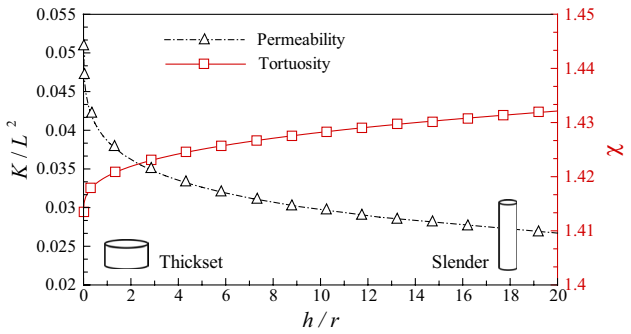

Fig. 6 Effect of micro-rod height-to-radius ratio on permeability and tortuosity for open-cell metal foam with a porosity of 0.90, a pore diameter of 1 mm and an interval of 13 μm for micro-rods

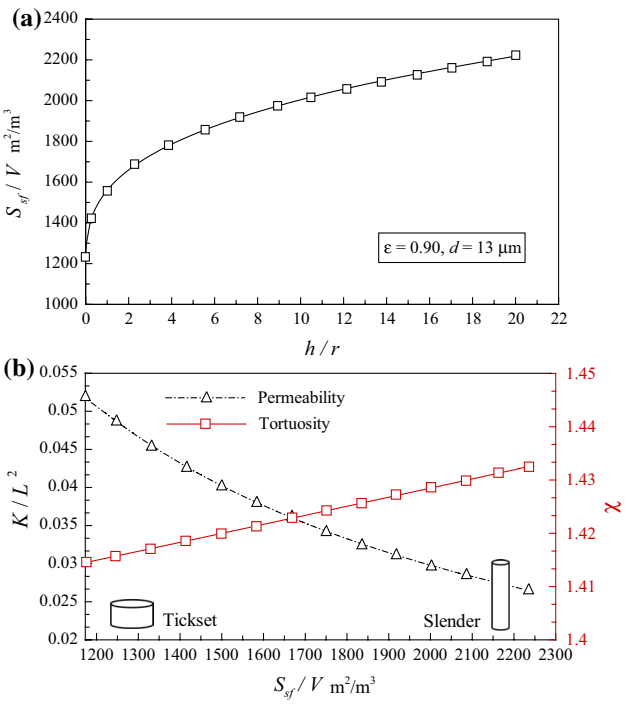

Fig. 7 **a** Specific area as a function of micro-rod height-to-radius ratio; **b** the effect of specific area on metal foam permeability. Note that the metal foam has a porosity of 0.90, a pore diameter of 1 mm and an interval of 13 μm for micro-rods

area) and flow features (flow tortuosity and permeability) will be investigated.

Figure 6 depicts the permeability as a function of micro-rod height-to-radius ratio. The metal foam has a porosity of 0.90, a pore diameter of 1 mm and an interval of 13 μm for micro-rods. To examine the influence of micro-rod height-to-radius ratio upon foam permeability, the volume for the total number of micro-rods is assumed to be constant. Upon the constant volume for a single rod, change in height-to-radius ratio will change the shape of the micro-rod; i.e., a lower ratio refers to a short and thick cylinder (namely thickset) and a higher one denotes a long and thin cylinder (namely slender). The permeability is monotonically decreased with the increase in height-to-radius ratio, and the value arrives at the one for metal foam without micro-roughness as h/r is approaching to zero, as shown in Fig. 6. This indicates that the slender rod has a more significant contribution to reducing the permeability than the thickset one. The decreased permeability may be explained that as the height-to-radius ratio increases, the micro-rods become higher, leading to a smaller equivalent pore diameter. The smaller the equivalent pore diameter, the lower permeability the metal foam has. Furthermore, from the flow condition point of view, a bigger height-to-radius ratio causes the surface rougher and thus increases the flow tortuosity (see Fig. 6 the red line), consequently leading to the reduced permeability.

Although the influences of microscopic parameters of micro-rods on metal foam permeability are discussed, a macroscopic parameter that can unify and represent the micro-features for porous media is needed. Specific area is the macroscopic parameter that can characterize the micro-scale porous media and is widely used in engineering applications. Figure 7a shows an increasing trend for the specific area as a function of micro-rod height-to-radius ratio. For a given volume of micro-rods, it can be seen that the case with slender rods has a much higher specific area than that with thickset ones. For instance, the specific area is increased by 17.6% as h/r is increased from 1 to 5. The relation between permeability and specific area for a porous medium is illustrated in Fig. 7b, where a dramatic decrease in permeability with the increased specific area is observed. This is expected since the larger specific area results in rougher surface, and thus inevitably lowers down the permeability. The flow tortuosity is increased with specific area, which can be also the reason why permeability is decreased with the increased specific area.

4 Conclusions

This study presents an analytical model for predicting the permeability of open-cell metal foams with surface covered by micro-roughness. Permeability is analytically expressed as a function of porosity, pore size, and geometric characteristics of micro-roughness, such as micro-rod radius, height and interval. Good agreement between the model predictions and the experimental measurements validates the present analytical model. It is demonstrated that the involvement of micro-roughness dramatically reduces the permeability of metal foam. An 84.03% reduction in permeability is observed as the micro-rod has a radius of 5 μm, a height of 30 μm and interval of 13 μm for a

selected porosity of 0.94. The increase in micro-rod radius/height or decrease in rod interval contributes significantly to the decrease in metal foam permeability. Besides, a higher micro-rod height-to-radius ratio (slender rod) makes the surface rougher than a lower one (thickset rod), and thus further reduces the permeability. The characterization of micro-roughness finally demonstrates that a larger specific area results in a lower permeability for porous media.

Acknowledgements This work was supported by the National Natural Science Foundation of China (51506160), China Post-Doctoral Science Foundation Project (2015M580845, 2016T90916), Shaanxi Province Post-Doctoral Science Foundation Project (2016BSHY-DZZ54) and the Beijing Key Lab of Heating, Gas Supply, Ventilating and Air Conditioning Engineering (NR2015K08 and NR2016K01).

References

Ahmed J, Pham C, Edouard D (2011) A predictive model based on tortuosity for pressure drop estimation in slim and fat foams. Chem Eng Sci 66:4771–4779

Bacchin P, Derekx Q, Veyret D, Glucina K, Moulin P (2014) Clogging of microporous channels networks: role of connectivity and tortuosity. Microfluid Nanofluid 17:85–96

Bhattacharya A, Calmidi V, Mahajan R (2002) Thermophysical properties of high porosity metal foams. Int J Heat Mass Transf 45:1017–1031

Burke DM, Morris MA, Holmes JD (2013) Chemical oxidation of mesoporous carbon foams for lead ion adsorption. Sep Purif Technol 104:150–159

Cai J, Yu B (2010) Prediction of maximum pore size of porous media based on fractal geometry. Fractals 18:417–423

Cai J, Yu B, Zou M, Mei M (2010a) Fractal analysis of surface roughness of particles in porous media. Chin Phys Lett 27:024705

Cai J, Yu B, Zou M, Mei M (2010b) Fractal analysis of invasion depth of extraneous fluids in porous media. Chem Eng Sci 65:5178–5186

Cai J, Hu X, Standnes DC, You L (2012) An analytical model for spontaneous imbibition in fractal porous media including gravity. Colloid Surf A Physicochem Eng Aspect 414:228–233

Cai J, San José MF, Martín MA, Hu X (2015) An introduction to flow and transport in fractal models of porous media Part II. Fractals 23:1502001

Despois JF, Mortensen A (2005) Permeability of open-pore microcellular materials. Acta Mater 53:1381–1388

Du Plessis JP, Masliyah JH (1988) Mathematical modelling of flow through consolidated isotropic porous media. Transp Porous Med 3:145–161

Du Plessis JP, Woudberg S (2008) Pore-scale derivation of the Ergun equation to enhance its adaptability and generalization. Chem Eng Sci 63:2576–2586

Du Plessis P, Montillet A, Comiti J, Legrand J (1994) Pressure drop prediction for flow through high porosity metallic foams. Chem Eng Sci 49:3545–3553

Du Plessis E, Woudberg S, du Plessis JP (2010) Pore-scale modelling of diffusion in unconsolidated porous structures. Chem Eng Sci 65:2541–2551

Dukhan N (2006) Correlations for the pressure drop for flow through metal foam. Exp Fluids 41:665–672

Edouard D, Lacroix M, Pham C, Mbodji M, Pham C (2008) Experimental measurements and multiphase flow models in solid SiC foam beds. AIChE J 54:2823–2832

Fourie JG, Du Plessis JP (2002) Pressure drop modelling in cellular metallic foams. Chem Eng Sci 57:2781–2789

Galindo FJ, Campo L, Pinho F, Van Bokhorst E, Hamersma P, Oliveira M, Alves M (2012) Microfluidic systems for the analysis of viscoelastic fluid flow phenomena in porous media. Microfluid Nanofluid 12:485–498

He ZQ, Zhan LY, Wang Q, Song S, Chen JM, Zhu KR, Xu XH, Liu WP (2011) Increasing the activity and stability of chemi-deposited palladium catalysts on nickel foam substrate by electrochemical deposition of a middle coating of silver. Sep Purif Technol 80:526–532

Hooman K, Dukhan N (2013) A theoretical model with experimental verification to predict hydrodynamics of foams. Transp Porous Med 100:393–406

Keh HJ, Hsu LY (2009) Diffusioosmotic flow of electrolyte solutions in fibrous porous media at arbitrary zeta potential and double-layer thickness. Microfluid Nanofluid 7:773–781

Kumar A, Reddy R (2003) Modeling of polymer electrolyte membrane fuel cell with metal foam in the flow-field of the bipolar/end plates. J Power Sources 114:54–62

Lacroix M, Nguyen P, Schweich D, Huu CP, Savin-Poncet S, Edouard D (2007) Pressure drop measurements and modeling on SiC foams. Chem Eng Sci 62:3259–3267

Lefebvre LP, Banhart J, Dunand D (2008) Porous metals and metallic foams: current status and recent developments. Adv Eng Mater 10:775–787

Liu R, Jiang Y, Li B, Yu L (2016) Estimating permeability of porous media based on modified Hagen-Poiseuille flow in tortuous capillaries with variable lengths. Microfluid Nanofluid 20:120

Lu TJ, Stone HA, Ashby MF (1998) Heat transfer in open-cell metal foams. Acta Mater 46:3619–3635

Lv Q, Wang E, Liu X, Wang S (2014) Determining the intrinsic permeability of tight porous media based on bivelocity hydrodynetics. Microfluid Nanofluid 16:841–848

Mu D, Liu Z-S, Huang C, Djilali N (2008) Determination of the effective diffusion coefficient in porous media including Knudsen effects. Microfluid Nanofluid 4:257–260

Ren Y, Wang K, Zhu B, Wang X, Wang X, Han F (2013) Synthesis of ZnO micro-rods on the cell walls of open celled Al foam and their effect on the sound absorption behavior. Mater Lett 91:242–244

Ren Y, Li Z, Han F (2014) Synthesis of Co3O4 Micro-needles on the cell walls and their effect on the sound absorption behavior of open cell al foam. Proc Mater Sci 4:191–195

Saini R, Kenny M, Barz DP (2015) Electroosmotic flow through packed beds of granular materials. Microfluid Nanofluid 19:693–708

Sen D, Nobes DS, Mitra SK (2012) Optical measurement of pore scale velocity field inside microporous media. Microfluid Nanofluid 12:189–200

Shou D, Fan J, Mei M, Ding F (2014) An analytical model for gas diffusion though nanoscale and microscale fibrous media. Microfluid Nanofluid 16:381–389

Straughan B, Harfash A (2013) Instability in Poiseuille flow in a porous medium with slip boundary conditions. Microfluid Nanofluid 15:109–115

Tawfik H, Hung Y, Mahajan D (2007) Metal bipolar plates for PEM fuel cell—a review. J Power Sources 163:755–767

Von Rickenbach J, Lucci F, Narayanan C, Eggenschwiler PD, Poulikakos D (2014) Multi-scale modelling of mass transfer limited heterogeneous reactions in open cell foams. Int J Heat Mass Transf 75:337–346

Weaire DL, Hutzler S (2001) The physics of foams. Oxford University Press, London

White FM, Corfield I (2006) Viscous fluid flow. McGraw-Hill Press, New York

Yang XH, Kuang J, Lu TJ, Han F, Kim T (2013a) A simplistic analytical unit cell based model for the effective thermal conductivity of high porosity open-cell metal foams. J Phys D Appl Phys 46:255302

Yang XH, Lu TJ, Kim T (2013b) A simplistic model for the tortuosity in two-phase close-celled porous media. J Phys D Appl Phys 46:125305

Yang XH, Lu TJ, Kim T (2014) An analytical model for permeability of isotropic porous media. Phys Lett A 378:2308–2311

Yang S, Liang M, Yu B, Zou M (2015) Permeability model for fractal porous media with rough surfaces. Microfluid Nanofluid 18:1085–1093

Yang XH, Wang WB, Yang C, Jin L, Lu TJ (2016) Solidification of fluid saturated in open-cell metallic foams with graded morphologies. Int J Heat Mass Transf 98:60–69

Yu B (2008) Analysis of flow in fractal porous media. Appl Mech Rev 61:050801

Yu B, Cheng P (2002) A fractal permeability model for bi-dispersed porous media. Int J Heat Mass Transf 45:2983–2993

Yu B, Li J (2004) A geometry model for tortuosity of flow path in porous media. Chin Phys Lett 21:1569

Yu B, Lee LJ, Cao H (2002) A fractal in-plane permeability model for fabrics. Polym Compos 23:201–221

Zhang J (2011) Lattice Boltzmann method for microfluidics: models and applications. Microfluid Nanofluid 10:1–28